11-8-2017

Cytochrome c as a Peroxidase: Activation of the Precatalytic Native State by H

Victor Yin

Gary S Shaw

Lars Konermann

Cytochrome *c* as a Peroxidase: Activation of the Pre-Catalytic Native State by H_2O_2-Induced Covalent Modifications

Victor Yin, Gary S. Shaw, and Lars Konermann*

Department of Chemistry and Department of Biochemistry, The University of Western Ontario, London, Ontario, N6A 5B7, Canada

* corresponding author

E-mail address of the corresponding author: konerman@uwo.ca

Funding was provided by the Natural Sciences and Engineering Research Council of Canada (DG 217080-2013 to LK) and the Canadian Institutes of Health Research (MOP 93520 to GSS).

Abstract: In addition to serving as respiratory electron shuttle, ferri-cytochrome *c* (cyt *c*) acts as a peroxidase, i.e., it catalyzes the oxidation of organic substrates by H_2O_2. This peroxidase function plays a key role during apoptosis. Typical peroxidases have a five-coordinate heme with a vacant distal coordination site that permits the iron center to interact with H_2O_2. In contrast, native cyt *c* is six-coordinate, as the distal coordination site is occupied by Met80. It thus seems counterintuitive that native cyt *c* would exhibit peroxidase activity. The current work scrutinizes the origin of this structure-function mismatch. Cyt *c*-catalyzed peroxidase reactions show an initial lag phase that is consistent with the *in situ* conversion of a pre-catalyst to an active peroxidase. Using mass spectrometry, we demonstrate the occurrence of cyt *c* self-oxidation in the presence of H_2O_2. The newly generated oxidized proteoforms are shown to possess significantly enhanced peroxidase activity. H_2O_2-induced modifications commence with oxidation of Tyr67, followed by permanent displacement of Met80 from the heme iron. The actual peroxidase activation step corresponds to subsequent side chain carbonylation, likely at Lys72/73. The Tyr67-oxidized / carbonylated protein has a vacant distal ligation site, and it represents the true peroxidase-active structure of cyt *c*. Subsequent self-oxidation eventually causes deactivation. It appears that this is the first report that identifies H_2O_2-induced covalent modifications as an essential component for the peroxidase activity of "native" cyt *c*.

Introduction

Cytochrome *c* (cyt *c*) is a highly conserved 12 kDa heme protein that transfers electrons in the respiratory chain. Cyt *c* can also catalyze the H_2O_2-induced oxidation of a wide range of substrates.[1-3] This peroxidase activity has attracted considerable attention due to its role during apoptosis (programmed cell death).[4-9] A key apoptotic pathway involves the production of H_2O_2 in mitochondria.[10,11] Cyt *c* utilizes this H_2O_2 to catalyze the oxidation of cardiolipin in the mitochondrial membrane.[4,5,12-14] The damaged membrane allows the release of pre-apoptotic factors into the cytoplasm, ultimately resulting in cell death.[4,6,7,15]

Like other peroxidases,[16-18] cyt *c* follows a mechanism where H_2O_2 reacts with the Fe(III) resting state to produce "Compound I", with a Fe(IV)=O heme and an adjacent radical. Subsequent H abstraction from organic substrates regenerates the resting state.[19] Reactions of the newly formed radicals with O_2 then yield stable oxidation products.[20,21] This cycle usually consumes external substrates, but it also oxidizes the protein and causes gradual deactivation.[22-25]

Classical peroxidases have a five-coordinate heme, where the sixth (distal) site is vacant or occupied by loosely bound water.[16,18,26] This five-coordinate structure allows for Fe-H_2O_2 interactions which are required for initiating the catalytic cycle.[6,8,13,14,26-28] Native cyt *c* is six-coordinate, with Met80 as distal ligand (Figure 1A).[29] It thus seems paradoxical that cyt *c* would be peroxidase-active.[14,30-33] A possible explanation invokes transiently formed five-coordinate conformers.[2,33-40] Rupture of the distal Met80-Fe bond by unfolding,[8,37] chemical,[2,31,32,35,41,42] or mutational[6,14,28,30,36,41,43-45] modifications enhances peroxidase activity.

The proximal His18-Fe contact in cyt *c* is quite robust, while the 70-85 Ω loop is flexible[39] and allows various distal ligation scenarios.[2,46] Basic pH produces "alkaline" conformers with Lys72, 73 or 79 as distal ligand (Figure 1B).[33,40,42,47,48] This transition can be

pushed into the neutral range by various means[2,35,42,46,49] that include Tyr67 modifications.[44,46,50] Similarly, cardiolipin binding[13,51,52] causes displacement of Met80 by Lys or His.[12,34,53,54]

Surprisingly, the aforementioned non-native conformers show enhanced peroxidase activity, despite their apparent lack of a vacant sixth coordination site.[6,13,26-28,35,42,49,55] Once again, catalysis may be facilitated by transiently populated five-coordinate forms.[2,33-40] However, alkaline iron ligation by Lys is more stable than the native Met80-Fe bond.[31,35,39,46] Alkaline conformers should thus have a lower peroxidase activity than native cyt *c*, which is opposite to the observed behavior.[15,35,42,49,55,56] Overall, it remains unclear why native cyt *c* and other six-coordinate variants possess apparent peroxidase activity.

Some catalyzed reactions (unrelated to peroxidases) exhibit an initial lag phase. Such behavior can have different mechanistic origins, but it often reflects the *in situ* activation of a pre-catalyst.[57-59] Intriguingly, a lag phase is also seen for cyt *c*-catalyzed peroxidase reactions.[14,40,60] The possible implications of this phenomenon have received surprisingly little attention. Cyt *c* kinetic analyses usually discard lag phase data, while focusing on the subsequent steady-state regime.[14,44,54,61] Contrary to prevailing views, there is a possibility that native cyt *c* does *not* exhibit substantial peroxidase activity, and that a potent peroxidase is formed only after H_2O_2-induced modifications. Such activated cyt *c* would likely be five-coordinate, as seen in certain peroxidase-enhanced mutants (Figure 1C).[14] The occurrence of an H_2O_2-induced activation step would imply that investigations conducted in the absence of H_2O_2 are unsuitable for deciphering the properties of peroxidase-active cyt *c*.

Here we address the issues outlined above by performing time-resolved experiments on the consequences of H_2O_2-cyt *c* interactions. We interrogate H_2O_2-induced structural changes by coupling catalase quenching assays with spectroscopic techniques, as well as mass spectrometry

(MS)-based peptide mapping, covalent labeling, and top-down assays. Our data suggest that unmodified cyt *c* exhibits minimal peroxidase activity. H_2O_2 causes highly selective covalent modifications that produce five-coordinate proteoforms with enhanced peroxidase activity. These findings resolve the apparent structure-function mismatch by uncovering a previously unrecognized H_2O_2-induced activation process.

Materials and Methods

Materials. Horse heart ferri-cyt *c*, guaiacol (o-methoxyphenol)[62], chloramine-T (N-chloro-4-toluol-sulfonamide)[63], and Girard's reagent T (GRT, carboxymethyl-trimethylammonium-hydrazide chloride)[64] were from Sigma (St. Louis, MO). Unless specified otherwise, solutions contained 10 μM cyt *c* in 65 mM aqueous potassium phosphate buffer at pH 7.4. The H_2O_2 concentration employed here (500 μM, unless noted otherwise) falls within the range used for earlier assays[14,40,60] and is physiologically relevant as the mitochondrial H_2O_2 concentration can reach ~10^{-4} M at the onset of apoptosis.[11] All experiments were conducted at 22 ± 2 °C.

Optical Spectroscopy. UV-Vis spectra were acquired on a Cary-100 instrument (Varian, Mississauga, ON). For measurements at 695 nm the protein concentration was raised to 40 μM. Peroxidase kinetics were measured by tracking the oxidation of 9 mM guaiacol in the presence of 1 μM cyt *c*. Reaction rates (μM guaiacol oxidized s^{-1}) were determined[62] with ε_{470} = 26.6 mM^{-1} cm^{-1} for the tetraguaiacol product. Circular dichroism (CD) spectra were recorded on a J-810 spectropolarimeter (JASCO, Easton, MD). For probing H_2O_2-induced structural changes, UV-Vis data were recorded on-line (20 s per spectrum). CD scans were slower (~20 min per spectrum), requiring quenching of the samples with 0.1 μM catalase prior to data acquisition.

Protein Samples. For MS, 100 μL aliquots were removed from the reaction mixture at selected time points, followed by catalase quenching. NMR samples were prepared identically, but in D_2O. In addition, NMR samples were concentrated to 100 μM using 10 kDa MWCO centrifuge filters (Millipore, Etobicoke, ON). Carbonyl labeling was performed by incubating 10 μM cyt *c* in buffer with 80 mM GRT[65] for 3 hours at room temperature. The reaction was halted by exchange into GRT-free buffer using 10 kDa MWCO filters.

NMR Spectroscopy. ^{1}H-NMR data were collected at 25˚C using a Varian Inova 600 MHz spectrometer using a spectral width of 50,000 Hz and an acquisition time of 0.4 s. 2,2-dimethyl-2-silapetane-5-sulphonate served as internal reference. A weak pre-saturation pulse was applied during the 0.1 s recycle delay to suppress the residual water signal. Data were zero filled to 132 K, processed using line broadening factors of 2.5 or 10 Hz, and baseline corrected.

Mass Spectrometry. MS was performed on a Synapt G2 ESI mass spectrometer coupled to a UPLC (Waters, Milford, MA). Intact cyt *c* was analyzed using a C4 desalting column. For top-down MS/MS, 16+ ions were quadrupole selected, followed by CID in Ar. [Fe(III) cyt *c* + 15H]$^{16+}$ isotope distributions[66] were simulated using ProteinProspector (UCSF). Tryptic peptides were generated using MS-grade modified trypsin (Promega, Madison, WI) in a 50:1 cyt *c*/trypsin ratio. Digests were incubated overnight at 37°C. Peptides were analyzed by LC/MS using a C18 column. Peptides were identified using data-dependent acquisition and MS^E. For quantitating oxidative modifications in tryptic peptides 2.5 μM bradykinin was added to each sample as internal standard after digestion.[67] Normalized peptide intensities $N(t)$ were calculated as a function of H_2O_2 incubation time t as $N(t) = I(t) / I_{brad}$, where $I(t)$ is the signal intensity of an

unmodified tryptic peptide at time t, and I_{brad} is the bradykinin intensity. In analogous fashion, N_{contr} data were generated for unoxidized control samples. The extent of oxidation can then be expressed as "fraction oxidized", $f_{OX}(t) = (1 - [N(t)/N_{contr}])$.[67] Monitoring the depletion of unoxidized peptides ensures robust f_{OX} data even if some of the products are difficult to detect.[67]

Results and Discussion

Peroxidase Kinetics. The peroxidase activity of cyt *c* can be probed by monitoring the oxidation of chromophoric substrates such as guaiacol in the presence of H_2O_2.[1,28,35,62,68] Without catalyst there was no evidence of product formation, whereas oxidation proceeded readily after cyt *c* addition (Figure 2). The guaiacol kinetics exhibited three stages (Figure 2): (i) a lag phase during which the rate gradually increased from ~zero, (ii) a linear steady-state region, and (iii) a region during which the rate declined. The third stage reflects oxidative deactivation of cyt *c* (Figure S1).[23,24] Lowering the H_2O_2 concentration slowed the overall progression (Figure S2). A lag phase was also seen for the oxidation of substrates other than guaiacol (Figure S3).

A lag phase in the peroxidase kinetics of cyt *c* has been reported previously,[14,40,60] but this phenomenon has received very little attention. One study[60] attributed the lag phase to Fe(II) → Fe(III) conversion, but this scenario can be excluded for the Fe(III) samples used here (Figure S4). We nonetheless agree with the basic conclusion of ref.[60] that the lag phase suggests some form of pre-catalyst activation.[57-59] Figures 2 and S3 still leave room for alternative explanations, but when considering the MS data discussed below it will become clear that covalent modifications are indeed required for converting cyt *c* to an active peroxidase.

Spectroscopic Evidence for H_2O_2-Induced Structural Changes. Upon exposing cyt *c* to H_2O_2 the CD amplitude at 222 nm decreased by ~30% within 20 min, implying a loss in α-helicity (Figure S5A).[69] A Soret shift from 409 nm to 406 nm indicated alterations in the heme environment, while a declining Soret intensity was caused by heme degradation (Figure S5B).[23,24,70,71] Disappearance of the 695 nm band (A695)[72] revealed rupture of the Met80-Fe bond (Figure S5C). A695 declined more rapidly than the Soret peak, implying that the loss of Met80 ligation is triggered by events other than heme degradation.

An important question is whether the loss of Met80 ligation is followed by the formation of alternative distal contacts. ^{1}H-NMR allows fingerprinting the Fe environment due to paramagnetic proton shifts.[40,42,46,73,74] After 5 min in H_2O_2 several ^{1}H signals associated with native cyt *c* had significantly dropped in intensity, including those of Met80 (Figure S6). This matches the UV-Vis-detected loss of Met80-Fe ligation (Figure S5C). The NMR spectra provided no evidence for alternative Fe ligation scenarios, e.g., distal Lys contacts would cause conspicuous peaks in the 12-25 ppm range.[46,74] No such signals were apparent in our NMR data, nor was there evidence that other ligands replace Met80. It is concluded that H_2O_2 triggers the formation of conformers with a vacant sixth coordination site. Considering that peroxidases require a five-coordinate heme,[6,8,13,14,26-28] our spectroscopic data strongly suggest that the peroxidase activity of cyt *c* arises from five-coordinate species produced in the presence of H_2O_2.

H_2O_2-Induced Modifications Probed by Mass Spectrometry. Intact protein mass spectra acquired during H_2O_2 incubation revealed a gradually declining signal amplitude (Figure 3A-D), concomitant with dramatic peak broadening (Figure 3E-H). The t = 0 spectrum displayed a single major isotope distribution corresponding to unmodified cyt *c*, denoted as "M0" in Figure

3E. After 10 min the mass distribution was split into numerous signals, arising from covalent oxidative modifications (M1, M2, M3, ..., Figure 3F-H). The spacing between successive M*i* species corresponded to mass differences of 14 - 16 Da. Similar patterns have previously been reported for other proteins after exposure to different types of oxidants.[22,32,75,76]

Peptide Mapping of Oxidation Patterns. LC-MS was applied to monitor H_2O_2-induced modifications via analyses of tryptic peptides. The resulting f_{OX} data (Figure S7A) were visualized as color maps (Figures 4, S7B). T13-T15 (residues 61-79) consistently stood out as the most heavily oxidized region. This region covers the distal side of the heme, i.e., the catalytically active region. Considering the critical role of the Met80-Fe bond for catalytic activity,[8,32,41,56,77] it might have been expected that the Met-80 containing T16 would be most strongly oxidized. However, T16 generally showed lower f_{OX} than T13-T15 (Figure 4).

H_2O_2-induced modifications were further characterized by subjecting tryptic peptides to tandem MS (Figure S8). Detected oxidation sites included Tyr48 (+16), Trp58 (+16,+32), Met80 (+16,+32) and a +32 Da shift within residues 33-35 (His-Gly-Leu). T5 could not be probed due to the heterogeneity of heme degradation products.[23,24,70,71] Surprisingly, we were unable to detect T13-T15 oxidation products after cyt *c* incubation in H_2O_2 (Figure 4). Chymotrypsin and GluC were tested as alternative proteases, but the results were inconclusive (data not shown). Oxidized T13-T15 peptides were readily observable after alternative treatments were performed as controls (Figure S9). This implies that H_2O_2 causes specific T13-T15 modifications that interfere with MS detection. The nature of these modifications will be discussed below.

The H_2O_2-induced oxidation patterns of Figure 4 are very different from those observed after exposing cyt *c* to free ·OH in bulk solution.[78] In the latter case, oxidation primarily affects

solvent-accessible residues.[20] In contrast, modifications formed under the conditions of the current work are heme-catalyzed,[19] such that buried sites adjacent to the porphyrin are particularly prone to oxidation.[22-25] Free ·OH is not involved in these peroxidase processes.[19]

Chemical Deconvolution. Several mechanistic aspects can be uncovered by examining the intact protein mass envelope. Figure 5A-C displays the mass distribution of unmodified cyt *c*. Oxidative modifications M1, M2, ... formed upon H_2O_2 exposure are highlighted in Figure 5D. The M1 population is of key interest because it carries the initial modifications. The M1 isotope envelope was ~50% wider than that of unmodified cyt *c*, and the center of M1 was shifted roughly -2 Da relative to a hypothetical [cyt *c* + O] species (Figure 5E). These characteristics imply that M1 encompasses different oxidation products with slightly different masses.

Chemical deconvolution was applied to tackle the heterogeneity of the H_2O_2-treated protein. GRT selectively tags reactive carbonyl groups formed by oxidation (i.e., not those of endogenous amides or carboxylates, Figure S10).[64,65,79,80] By shifting carbonylated species into a mass range that differs from that of non-carbonylated forms, GRT labeling reveals proteins carrying other types of modifications. Without H_2O_2 treatment cyt *c* did not incorporate GRT (Figure S11D). In contrast, extensive GRT labeling took place for M1, M2, ... formed in the presence of H_2O_2 (Figure 5I). This observation reveals that H_2O_2 causes cyt *c* carbonylation, consistent with immunological data.[81] The extent of carbonylation increased with H_2O_2 exposure time (Figure S11). Reaction products M1, M2, ... tagged with one or two GRT moieties were clearly discernible in the spectra (Figures 5I, S12). The relatively low signal intensity of these products likely reflects the aggregation propensity of carbonylated proteins.[82]

In addition to unmodified cyt *c* (M0), carbonyl-depleted cyt *c* showed "M1" as the only major signal (Figure 5G). The centroid of this carbonyl-depleted M1 was shifted by roughly +2 Da relative to the original M1 (Figures 6E, H). We will refer to this sub-population as M1*. Comparison with a simulated isotope envelope reveals that M1* primarily consists of proteins with the composition [cyt *c* + O] (Figure 5H).

The aforementioned findings demonstrate that M1 (Figure 5E) comprises [cyt *c* + O], along with carbonylated species that are 1 to 2 Da lower in mass. Lys conversion to aminoadipic semialdehyde ($R\text{-}CH_2\text{-}NH_2 \rightarrow R\text{-}CHO$) is the only documented carbonylation pathway with a mass shift of -1 Da.[20,79] Thus, we propose that M1 contains [cyt *c* + O] where 0, 1, or 2 of the 19 Lys side chains have undergone carbonylation. Tyr dimerization (-2 Da)[83] and other crosslinking modifications[20,79] in M1 can be excluded, because they would not convey GRT reactivity. Thus, the various oxidative modifications detected by peptide mapping (at Tyr48, Trp58, Met80 etc., see above) must reside in the more highly oxidized species M*i*, with $i > 1$. Likely, these highly oxidized species are also subject to Tyr dimerization, as suggested in previous work.[81,83]

Figure 5 also provides information regarding the temporal sequence of oxidation events. [cyt *c* + O] is susceptible to carbonylation, seen from disappearance of -1 and -2 Da mass shifts by GRT labeling, and from the formation of [M1+GRT] and [M1+2GRT] (Figures 5I, S11). In contrast, M0 is effectively inert against carbonylation, evident from the fact that neither H_2O_2 nor GRT treatment affect the M0 mass distribution (Figure 5E, H), and from the lack of a discernible [M0 + GRT] signal in Figure 5I. Hence, carbonylation occurs *after* an initial +O modification.

The carbonyl-depleted and the carbonylated sub-populations show major differences in their degree of self-oxidation, which serves as a proxy for the level of peroxidase activity. The carbonyl-depleted sub-population is dominated by M1* (incorporation of a single oxygen, Figure

6A). In contrast, carbonylated cyt *c* has its maximum at [M2+GRT] with major contributions from [M3+GRT] and beyond (with 2, 3, ... incorporated oxygens, Figure 6B). Because these oxidative modifications are heme-mediated,[22-25] the fact that carbonylated cyt *c* exhibits more extensive self-oxidation, implies that carbonylation enhances peroxidase activity relative to unmodified cyt *c* and [cyt *c* + O]. In other words, Figure 6 provides unequivocal proof that chemical modifications cause peroxidase activation of cyt *c*, i.e., the transition of a low activity catalyst to the active enzyme. Our data imply that this activation follows a sequential mechanism, with incorporation of a single oxygen as the initial step. The [cyt *c* + O] formed in this way retains a low peroxidase activity, similar to that of the unmodified protein. Peroxidase activation takes place upon subsequent carbonylation.

Top-down MS. To pinpoint the initial [cyt *c* + O] modification(s) we performed top-down experiments, i.e., tandem MS without prior protein digestion.[84] This approach allowed the interrogation of specific species within the heterogeneous mix formed during H_2O_2 exposure. Top-down data (Figure S13) were acquired for three precursor ions, the M0 unmodified control (Figure 5B), M1 (Figure 5E), and carbonyl-depleted M1* (Figure 5H). The *b* and *y* fragments provided complete sequence coverage (Figure 7A). Dissociation of both M1 and M1* resulted in unmodified C-terminal fragments up to y_{37}, whereas a +16 Da shift was seen from y_{38} onwards (Figure 7B). This pattern identifies Tyr67 as the oxidation site in [cyt *c* + O]. Other oxidation sites were absent, revealing that M1* is just a single proteoform. The top-down identification of Tyr67 oxidation is also consistent with the peptide data of Figure 4, which mapped the most prevalent early modification to residues 61-79.

Unfortunately, top-down fragmentation did not reveal the nature of carbonylation sites, as none of the M1 fragments displayed mass shifts related to Lys carbonylation (or other non-Tyr67 oxidation events). GRT labeling revealed that M1 represents a mix of carbonylated and non-carbonylated species. Evidently, the fragmentation of carbonylated proteins was suppressed in our top-down experiments. We attribute this effect to the inability of carbonylated Lys to bear charge, thereby inhibiting the gas phase dissociation of amide bonds[85,86] or favoring dissociation pathways that do not conform to canonical *b*/*y* patterns.[87] Peptide mapping using trypsin, chymotrypsin, and GluC was applied as outlined above, but unfortunately those experiments also did not yield direct information regarding the location of carbonylation sites.

Despite our inability to directly identify the nature of carbonylation sites in M1, there is evidence to suggest that Lys72/73 are primarily affected. Carbonylation of these residues explains the lack of detectable oxidized peptides in the T13-T15 region. Specifically, the high f_{OX} of T15 at early times (Figure 4) likely reflects a missed tryptic cleavage due to Lys73 carbonylation. Also, Lys72/Lys73 are known to adopt positions close to the heme in "alkaline" cyt *c*,[2,40,42,44,46-50] particularly after Tyr67 modifications.[35] The proximity to the reactive iron makes Lys72/Lys73 prime candidates for oxidative modifications. Consistent with this view, the spectroscopic properties of H_2O_2-activated cyt *c* (at $t \approx 5$ min, Figure S5) are close to those of "alkaline" Tyr67Arg cyt *c*.[46] Similarities include a Soret maximum at 406 nm, the shape of the CD spectrum with a minimum at ~206 nm, and loss of A695. The 406 nm Soret signal is compatible with distal ligation by OH^-/H_2O (after H_2O_2-activation) or by Lys (for Tyr67Arg).[35]

It is instructive to consider the viability of alternative scenarios, where M1 represents a mix of two independently formed products, i.e., [cyt *c* + O] (Tyr67 oxidized, +16 Da) and [cyt *c* + O - 2H] (aliphatic ketone, +14 Da). In such a case Figure 6 would imply that the +14 Da

species is highly prone to self-oxidation, whereas Tyr67 oxidation protects the protein against additional modifications. It is difficult to envision such a scenario because (i) Tyr67 modifications generally enhance (rather than inhibit) peroxidase activity.[35,44,46,50] (ii) If Tyr67 were to inhibit self-oxidation M1* should accumulate after extended H_2O_2 exposure, in contradiction with the spectra of Figure 3. (iii) +14 Da products are generally disfavored relative to other modifications,[20,79] while Lys carbonylation is highly prevalent during metal-catalyzed oxidation.[88] (iv) The top-down detection of +14 Da modifications should be straightforward; our data did not provide any evidence of such species. All these points argue against the presence of +14 Da modifications in M1, reinforcing the view that Tyr67 oxidation leads to an on-pathway intermediate (M1*) that undergoes subsequent Lys carbonylation to form M1.

Peroxidase Activation Mechanism of Cyt *c*. From the data presented above we can propose a model for the H_2O_2-induced peroxidase activation of cyt *c* (Figure 8). The native state M0 has low peroxidase activity because the distal coordination site is occupied by Met80, restricting interactions of the iron center with H_2O_2. The initial modification en route towards the active state is Tyr67 oxidation (to 3,4- or 2,4-dihydroxyphenylalanine[20]). This reaction likely takes place in a heme-catalyzed fashion,[89] facilitated by transient opening events of the 70-85 Ω loop[8,9,30] which represents the most dynamic cyt *c* region (Figure 1).[39] A Tyr67 radical formed in the presence of H_2O_2[89,90] may be an intermediate of this oxidation step. Tyr67 modifications are known to destabilize the Met80-Fe bond due to involvement of the Tyr side chain in packing interactions and H-bonding. These conditions favor distal heme ligation by Lys72/73.[44,46,50] Our data suggest that an analogous ligand displacement takes place after Tyr67 oxidation, producing M1* where Lys72/73 compete with Met80 for iron ligation. M1* transiently accumulates to no

more than ~10% of the total protein population (Figure 6). The lack of discernible Lys-specific ^{1}H-NMR signals (Figure S6) indicates that iron contacts with Lys72/73 in the M1* state remain fluctional, while the proximity of Lys72/73 to the redox-active heme triggers carbonylation. Carbonylated Lys is no longer capable of iron ligation, leaving behind a vacant distal coordination site. The five-coordinate M1 produced in this way represents the nascent peroxidase-active state of cyt *c*. Peroxidase activity is likely retained while additional oxidation events affect Met80, Tyr48, Trp58 and other residues (corresponding to M2, M3, ...). Activity is gradually lost as more and more of the protein is affected by oxidation.

The modification steps of Figure 8 require access of H_2O_2 and O_2 to the protein interior. We envision that this access is provided by conformational fluctuations, consistent with earlier proposals.[2,33-40] Such fluctuations will be particularly important for facilitating the initial steps, i.e. M0 $\rightarrow$ M1* $\rightarrow$ M1. However, much of the earlier literature implicitly assumed that native state fluctuations *per se* might produce a five-coordinate population that is entirely responsible for the "native state" peroxidase activity. Our observations demonstrate that the peroxidase activity of unmodified native cyt *c* is low, and that significant substrate turnover takes place only after carbonylation.

Conclusions

Previous studies did not comprehensively answer the question why native cyt *c*, with its six-coordinate iron, possesses apparent peroxidase activity. The present work resolves this conundrum by attributing much of the peroxidase activity to five-coordinate species formed in the presence of H_2O_2. The conversion from a pre-catalyst to peroxidase-active cyt *c* is consistent with the observation of a lag phase during substrate oxidation.[14,40,60]

Various reasons may have contributed to the fact that the H_2O_2-induced activation of cyt *c* has been overlooked in the past. Many earlier studies characterized wild type and mutant proteins *ex situ*, without considering the possibility of H_2O_2-induced, functionally relevant alterations. Also, H_2O_2 produces a mix of transient proteoforms that are difficult to characterize by most techniques. Here we approached the problem from a new angle by interrogating catalase-quenched samples in a time-resolved fashion using optical techniques and MS.

It is tempting to speculate on the implications of our findings for the role of cyt *c* during apoptosis. Our *in vitro* data suggest that cyt *c* within mitochondria might also adopt its peroxidase-active state only after oxidative modifications. Specifically, cardiolipin-bound cyt *c* with Lys or His ligation[12,34,53,54] likely does not represent a form that is highly peroxidase-active. Instead, these hexa-coordinate species may be analogous to M1* (Figure 8), requiring oxidative modifications to free up the distal coordination site prior to becoming an active catalyst. Similarly, engineered six-coordinate constructs might enter the sequence of Figure 8 at the M1* stage, skipping the initial oxidation event, and thereby providing an explanation for their enhanced apparent peroxidase activity.[6,13,26-28,35,42,49,55]

Acknowledgements. We thank Lee-Ann Briere for assistance with the optical experiments which were conducted in the UWO Biomolecular Interactions and Conformations Facility.

Supporting Information Available. Additional figures as noted in the text. This material is available free of charge via the Internet at http://pubs.acs.org.

References

(1) Vazquez-Duhalt, R. *J. Mol. Catal. B* **1999**, *7*, 241-249.
(2) Hannibal, L.; Tomasina, F.; Capdevila, D. A.; Demicheli, V.; Tórtora, V.; Alvarez-Paggi, D.; Jemmerson, R.; Murgida, D. H.; Radi, R. *Biochemistry* **2016**, *55*, 407-428.
(3) Dunford, H. B. *Peroxidases and Catalases: Biochemistry, Biophysics, Biotechnology, and Physiology*; 2nd ed. John Wiley & Sons: Hoboken, N.J, 2010.
(4) Kagan, V. E.; Tyurin, V. A.; Jiang, J.; Tyurina, Y. Y.; Ritov, V. B.; Amoscato, A. A.; Osipov, A. N.; Belikova, N. A.; Kapralov, A. A.; Kini, V.; Vlasova, I. I.; Zhao, Q.; Zou, M.; Di, P.; Svistunenko, D. A.; Kurnikov, I. V.; Borisenko, G. G. *Nat. Chem. Biol.* **2005**, *1*, 223-232.
(5) Jiang, X.; Wang, X. *Annu. Rev. Biochem.* **2004**, *73*, 87-106.
(6) Godoy, L. C.; Muñoz-Pinedo, C.; Castro, L.; Cardaci, S.; Schonhoff, C. M.; King, M.; Tórtora, V.; Marín, M.; Miao, Q.; Jiang, J. F.; Kapralov, A. A.; Jemmerson, R.; Silkstone, G. G.; Patel, J. N.; Evans, J. E.; Wilson, M. l. T.; Green, D. R.; Kagan, V. E.; Radi, R.; Mannick, J. B. *Proc. Natl. Acad. Sci. U.S.A.* **2009**, *106*, 2653-2658.
(7) Yu, X.; Acehan, D.; Menetret, J. F.; Booth, C. R.; Ludtke, S. J.; Riedl, S. J.; Shi, Y.; Wang, X.; Akey, C. W. *Structure* **2005**, *13*, 1725-1735.
(8) Bren, K. L.; Raven, E. L. *Science* **2017**, *356*, 1236-1236.
(9) Mara, M. W.; Hadt, R. G.; Reinhard, M. E.; Kroll, T.; Lim, H.; Hartsock, R. W.; Alonso-Mori, R.; Chollet, M.; Glownia, J. M.; Nelson, S.; Sokaras, D.; Kunnus, K.; Hodgson, K. O.; Hedman, B.; Bergmann, U.; Gaffney, K. J.; Solomon, E. I. *Science* **2017**, *356*, 1276-1280.
(10) Lee, S.; Tak, E.; Lee, J.; Rashid, M. A.; Murphy, M. P.; Ha, J.; Kim, S. S. *Cell Res.* **2011**, *21*, 817-834.
(11) Giorgio, M.; Trinei, M.; Migliaccio, E.; Pelicci, P. G. *Nat. Rev. Mol. Cell Biol.* **2007**, *8*, 722A-728.
(12) Bradley, J. M.; Silkstone, G.; Wilson, M. T.; Cheesman, M. R.; Butt, J. N. *J. Am. Chem. Soc.* **2011**, *133*, 19676-19679.
(13) Abe, M.; Niibayashi, R.; Koubori, S.; Moriyama, I.; Miyoshi, H. *Biochemistry* **2011**, *50*, 8383-8391.
(14) McClelland, L. J.; Mou, T.-C.; Jeakins-Cooley, M. E.; Sprang, S. R.; Bowler, B. E. *Proc. Natl. Acad. Sci. U.S.A.* **2014**, *111*, 6648-6653.
(15) Kitt, J. P.; Bryce, D. A.; Minteer, S. D.; Harris, J. M. *J. Am. Chem. Soc.* **2017**.
(16) Veitch, N. C. *Phytochem.* **2004**, *65*, 249-259.
(17) Rodriguez Maranon, M. J.; Mercier, D.; van Huystee, R. B.; Stillman, M. J. *Biochem. J.* **1994**, *301 (Pt 2)*, 335-341.
(18) Volkov, A. N.; Nicholls, P.; Worrall, J. A. R. *Biochim. Biophys. Acta.* **2011**, *1807*, 1482-1503.
(19) Lawrence, A.; Jones, C. M.; Wardman, P.; Burkitt, M. J. *J. Biol. Chem.* **2003**, *278*, 29410-29419.
(20) Xu, G.; Chance, M. R. *Chem. Rev.* **2007**, *107*, 3514-3543.
(21) Von Sonntag, C.; Schuchmann, H. P. *Angew. Chem.-Int. Edit. Engl.* **1991**, *30*, 1229-1253.
(22) Kathiresan, M.; English, A. M. *Chem. Sci.* **2017**, *8*, 1152-1162.
(23) Florence, T. M. *J. Inorg. Biochem.* **1985**, *23*, 131-141.
(24) Villegas, J. A.; Mauk, A. G.; Vazquez-Duhalt, R. *Chem. Biol.* **2000**, *7*, 237-244.
(25) Gray, H. B.; Winkler, J. R. *Proc. Natl. Acad. Sci. U. S. A.* **2015**, *112*, 10920-10925.

(26) Hersleth, H.-P.; Ryde, U.; Rydberg, P.; Görbitz, C. H.; Andersson, K. K. *J. Inorg. Biochem.* **2006**, *100*, 460-476.
(27) Diederix, R. E. M.; Ubbink, M.; Canters, G. W. *ChemBioChem* **2002**, *3*, 110-112.
(28) Wang, Z.-H.; Lin, Y.-W.; Rosell, F. I.; Ni, F.-Y.; Lu, H.-J.; Yang, P.-Y.; Tan, X.-S.; Li, X.-Y.; Huang, Z.-X.; Mauk, A. G. *ChemBioChem* **2007**, *8*, 607-609.
(29) Bushnell, G. W.; Louie, G. V.; Brayer, G. D. *J. Mol. Biol.* **1990**, *214*, 585-595.
(30) Moreno-Beltran, B.; Guerra-Castellano, A.; Diaz-Quintana, A.; Del Conte, R.; Garcia-Maurino, S. M.; Diaz-Moreno, S.; Gonzalez-Arzola, K.; Santos-Ocana, C.; Velazquez-Campoy, A.; De la Rosa, M. A.; Turano, P.; Diaz-Moreno, I. *Proc. Natl. Acad. Sci. U. S. A.* **2017**, *114*, E3041-E3050.
(31) Capdevila, D. A.; Oviedo Rouco, S.; Tomasina, F.; Tortora, V.; Demicheli, V.; Radi, R.; Murgida, D. H. *Biochemistry* **2015**, *54*, 7491−7504.
(32) Chen, Y.-R.; Deterding, L. J.; Sturgeon, B. E.; Tomer, K. B.; Mason, R. P. *J. Biol. Chem.* **2002**, *277*, 29781-29791.
(33) Nold, S. M.; Lei, H.; Mou, T.-C.; Bowler, B. E. *Biochemistry* **2017**, *56*, 3358–3368.
(34) Milazzo, L.; Tognaccini, L.; Howes, B. D.; Sinibaldi, F.; Piro, M. C.; Fittipaldi, M.; Baratto, M. C.; Pogni, R.; Santucci, R.; Smulevich, G. *Biochemistry* **2017**, *56*, 1887-1898.
(35) Amacher, J. F.; Zhong, F. F.; Lisi, G. P.; Zhu, M. Q.; Alden, S. L.; Hoke, K. R.; Madden, D. R.; Pletneva, E. V. *J. Am. Chem. Soc.* **2015**, *137*, 8435-8449.
(36) Karsisiotis, A. I.; Deacon, O. M.; Wilson, M. T.; Macdonald, C.; Blumenschein, T. M. A.; Moore, G. R.; Worrall, J. A. R. *Sci Rep* **2016**, *6*, 30447.
(37) Diederix, R. E. M.; Ubbink, M.; Canters, G. W. *Biochemistry* **2002**, *41*, 13067-13077.
(38) Sutin, N.; Yandell, J. K. *J. Biol. Chem.* **1972**, *247*, 6932-6936.
(39) Xu, Y.; Mayne, L.; Englander, S. W. *Nat. Struct. Biol.* **1998**, *5*, 774-778.
(40) García-Heredia, J. M.; Díaz-Moreno, I.; Nieto, P. M.; Orzáez, M.; Kocanis, S.; Teixeira, M.; Pérez-Payá, E.; Díaz-Quintana, A.; De la Rosa, M. A. *Biochim. Biophys. Acta* **2010**, *1797*, 981-993.
(41) Wang, Z.; Ando, Y.; Nugraheni, A. D.; Ren, C.; Nagao, S.; Hirota, S. *Mol. Biosyst.* **2014**, *10*, 3130-3137.
(42) Abriata, L. A.; Cassina, A.; Tortora, V.; Marin, M.; Souza, J. M.; Castro, L.; Vila, A. J.; Radi, R. *J. Biol. Chem.* **2009**, *284*, 17-26.
(43) Josephs, Tracy M.; Morison, Ian M.; Day, Catherine L.; Wilbanks, Sigurd M.; Ledgerwood, Elizabeth C. *Biochem. J.* **2014**, *458*, 259-265.
(44) Tognaccini, L.; Ciaccio, C.; D'Oria, V.; Cervelli, M.; Howes, B. D.; Coletta, M.; Mariottini, P.; Smulevich, G.; Fiorucci, L. *J. Inorg. Biochem.* **2016**, *155*, 56-66.
(45) Ciaccio, C.; Tognaccini, L.; Battista, T.; Cervelli, M.; Howes, B. D.; Santucci, R.; Coletta, M.; Mariottini, P.; Smulevich, G.; Fiorucci, L. *J. Inorg. Biochem.* **2017**, *169*, 86-96.
(46) Gu, J.; Shin, D.-W.; Pletneva, E. V. *Biochemistry* **2017**, *56*, 2950−2966.
(47) Assfalg, M.; Bertini, I.; Dolfi, A.; Turano, P.; Mauk, A. G.; Rosell, F. I.; Gray, H. B. *J. Am. Chem. Soc.* **2003**, *125*, 2913-2922.
(48) Döpner, S.; Hildebrandt, P.; Rosell, F. I.; Mauk, A. G. *J. Am. Chem. Soc.* **1998**, *120*, 11246-11255.
(49) Garcia-Heredia, J. M.; Diaz-Quintana, A.; Salzano, M.; Orzaez, M.; Perez-Paya, E.; Teixeira, M.; De la Rosa, M. A.; Diaz-Moreno, I. *J. Biol. Inorg. Chem.* **2011**, *16*, 1155-1168.
(50) Ying, T.; Wang, Z.-H.; Lin, Y.-W.; Xie, J.; Tan, X.; Huang, Z.-X. *Chem. Commun.* **2009**, 4512-4514.

(51) Kagan, V. E.; Bayır, H. A.; Belikova, N. A.; Kapralov, O.; Tyurina, Y. Y.; Tyurin, V. A.; Jiang, J.; Stoyanovsky, D. A.; Wipf, P.; Kochanek, P. M.; Greenberger, J. S.; Pitt, B.; Shvedova, A. A.; Borisenko, G. G. *Free Radic. Biol. Med.* **2009**, *46*, 1439-1453.
(52) Serpas, L.; Milorey, B.; Pandiscia, L. A.; Addison, A. W.; Schweitzer-Stenner, R. *J. Phys. Chem. B* **2016**, *120*, 12219−12231.
(53) Ranieri, A.; Millo, D.; Di Rocco, G.; Battistuzzi, G.; Bortolotti, C. A.; Borsari, M.; Sola, M. *J. Biol. Inorg. Chem.* **2015**, *20*, 531-540.
(54) Yanamala, N.; Kapralov, A. A.; Djukic, M.; Peterson, J.; Mao, G. W.; Klein-Seetharaman, J.; Stoyanovsky, D. A.; Stursa, J.; Neuzil, J.; Kagan, V. E. *J. Biol. Chem.* **2014**, *289*.
(55) Belikova, N. A.; Vladimirov, Y. A.; Osipov, A. N.; Kapralov, A. A.; Tyurin, V. A.; Potapovich, M. V.; Basova, L. V.; Peterson, J.; Kurnikov, I. V.; Kagan, V. E. *Biochemistry* **2006**, *45*, 4998-5009.
(56) Capdevila, D. A.; Marmisolle, W. A.; Tomasina, F.; Demicheli, V.; Portela, M.; Radi, R.; Murgida, D. H. *Chem. Sci.* **2015**, *6*, 705-713.
(57) Widegren, J. A.; Finke, R. G. *J. Mol. Catal. A* **2003**, *198*, 317-341.
(58) Haw, J. F.; Song, W. G.; Marcus, D. M.; Nicholas, J. B. *Acc. Chem. Res.* **2003**, *36*, 317-326.
(59) Wunder, S.; Lu, Y.; Albrecht, M.; Ballauff, M. *ACS Catal.* **2011**, *1*, 908-916.
(60) Radi, R.; Thomson, L. M.; Rubbo, H.; Prodanov, E. *Arch. Biochem. Biophys.* **1991**, *288*, 112-117.
(61) Capdevila, D. A.; Alvarez-Paggi, D.; Castro, M. A.; Tortora, V.; Demicheli, V.; Estrin, D. A.; Radi, R.; Murgida, D. H. *Chem. Commun.* **2014**, *50*, 2592-2594.
(62) Baldwin, D. A.; Marques, H. M.; Pratt, J. M. *J. Inorg. Biochem.* **1987**, *30*, 203-217.
(63) Pande, J.; Kinnally, K.; Thallum, K. K.; Verma, B. C.; Myer, Y. P.; Rechsteiner, L.; Bosshard, H. R. *J. Protein Chem.* **1987**, *6*, 295-319.
(64) Yang, Y.; Stella, C.; Wang, W. R.; Schoneich, C.; Gennaro, L. *Anal. Chem.* **2014**, *86*, 4799-4806.
(65) Mirzaei, H.; Regnier, F. *J. Chromatogr. A* **2006**, *1134*, 122-133.
(66) He, F.; Hendricksen, C. L.; Marshall, A. G. *J. Am. Soc. Mass Spectrom.* **2000**, *11*, 120-126.
(67) Stocks, B. B.; Konermann, L. *Anal. Chem.* **2009**, *81*, 20-27.
(68) Matsui, T.; Ozaki, S.-i.; Watanabe, Y. *J. Am. Chem. Soc.* **1999**, *121*, 9952-9957.
(69) Chen, Y.; Yang, J. T.; Martinez, H. M. *Biochemistry* **1972**, *22*, 4120-4131.
(70) Lan, W.; Wang, Z.; Yang, Z.; Ying, T.; Zhang, X.; Tan, X.; Liu, M.; Cao, C.; Huang, Z.-X. *PLoS ONE* **2014**, *9*, e107305.
(71) Nagababu, E.; Rifkind, J. M. *Antioxid. Redox Signal.* **2004**, *6*, 967-978.
(72) Kaminsky, L. S.; Miller, V. J.; Davison, A. J. *Biochemistry* **1973**, *12*, 2215-2221.
(73) Feng, Y. Q.; Roder, H.; Englander, S. W. *Biophys. J.* **1990**, *57*, 15-22.
(74) Russell, B. S.; Melenkivitz, R.; Bren, K. L. *Proc. Natl. Acad. Sci. U. S. A.* **2000**, *97*, 8312-8317.
(75) Lim, J.; Vachet, R. W. *Anal. Chem.* **2004**, *76*, 3498-3504.
(76) Gau, B. C.; Sharp, J. S.; Rempel, D. L.; Gross, M. L. *Anal. Chem.* **2009**, *81*, 6563–6571.
(77) Birk, A. V.; Chao, W. M.; Liu, S. Y.; Soong, Y.; Szeto, H. H. *Biochim. Biophys. Acta* **2015**, *1847*, 1075-1084.
(78) Stocks, B. B.; Konermann, L. *J. Mol. Biol.* **2010**, *398*, 362-373.
(79) Møller, I. M.; Rogowska-Wrzesinska, A.; Rao, R. S. P. *J. Proteomics* **2011**, *74*, 2228-2242.
(80) Artemenko, K.; Mi, J.; Bergquist, J. *Free Radical Res.* **2015**, *49*, 477-493.
(81) Kim, N. H.; Jeong, M. S.; Choir, S. Y.; Kang, J. H. *Mol. Cells* **2006**, *22*, 220-227.

(82) de Graff, A. M. R.; Hazoglou, M. J.; Dill, K. A. *Structure* **2016**, *24*, 329-336.
(83) Tew, D.; Demontellano, P. R. O. *J. Biol. Chem.* **1988**, *263*, 17880-17886.
(84) Siuti, N.; Kelleher, N. L. *Nat. Methods* **2007**, *4*, 817-821.
(85) Dongré, A. R.; Jones, J. L.; Somogyi, Á.; Wysocki, V. H. *J. Am. Chem. Soc.* **1996**, *118*, 8365-8374.
(86) Greer, S. M.; Holden, D. D.; Fellers, R.; Kelleher, N. L.; Brodbelt, J. S. *J. Am. Soc. Mass Spectrom.* **2017**, *28*, 1587-1599.
(87) Paizs, B.; Suhai, S. *Mass Spectrom. Rev.* **2005**, *24*, 508-548.
(88) Temple, A.; Yen, T.-Y.; Gronert, S. *J. Am. Soc. Mass Spectrom.* **2006**, *17*, 1172-1180.
(89) Kapralov, A. A.; Yanamala, N.; Tyurina, Y. Y.; Castro, L.; Samhan-Arias, A.; Vladimirov, Y. A.; Maeda, A.; Weitz, A. A.; Peterson, J.; Mylnikov, D.; Demicheli, V.; Tortora, V.; Klein-Seetharaman, J.; Radi, R.; Kagan, V. E. *Biochim. Biophys. Acta* **2011**, *1808*, 2147-2155.
(90) Qian, S. Y.; Chen, Y.-R.; Deterding, L. J.; Fann, Y. C.; Chignell, C. F.; Tomer, K. B.; Mason, R. P. *Biochem. J.* **2002**, *363*, 281-288.

Figure Captions

Figure 1. Cyt *c* crystal structures. The 70-85 Ω-loop is depicted in magenta, key residues are highlighted in cyan, iron is displayed in red. (A) Native equine wild-type with Met80-Fe ligation (pdb: 1hrc).[29] (B) Alkaline conformer with Lys73-Fe ligation (yeast K72A/T78C/K79G/C102S, pdb: 4q5p.)[35] (C) Distally de-ligated form (yeast K72A/C102S, pdb: 4mu8).[14]

Figure 2. Peroxidase activity of 1 μM cyt *c* measured by guaiacol oxidation (9 mM) in the presence of 500 μM H_2O_2 in phosphate buffer at pH 7.4. A fit to the linear region (solid gray line) yields a reaction rate of 0.027 μM s^{-1}.

Figure 3. (A-D): Cyt *c* mass spectra acquired after varying H_2O_2 incubation times. (E-H): 16+ charge state region. M0 denotes unmodified protein. M1, M2, ... refers to oxidatively modified forms. Protein (10 μM) and H_2O_2 (500 μM) were incubated in phosphate buffer at pH 7.4.

Figure 4. (A) Tryptic peptide mapping, displaying the extent of oxidative modifications as a function of H_2O_2 incubation time. Colors indicate the fraction oxidized, f_{OX}, ranging from blue (little oxidation) to red (heavily oxidized). Met80 is highlighted as spheres. Regions for which no structural data were obtained are colored grey (sequence coverage 89%). (B) f_{OX} data for t = 5 min mapped to the cyt *c* sequence Detected tryptic peptides are annotated as T1, T4, etc. Peptides T9-10, T13-14, and T18-20 arise from missed cleavage sites. T5 includes the heme.

Figure 5. Mass spectra of the 16+ charge state for unmodified cyt *c* (A-C), after 5 min in H_2O_2 (D-F), and after 5 min in H_2O_2 with subsequent GRT labeling (G-I). Column 2 shows close-ups of the region comprising M0 (unmodified protein) and M1 (first modification peak), with

simulated isotope envelopes for cyt *c* and [cyt *c* + O]. Column 3 shows the GRT-labeled M*i* forms. Carbonyl-depleted M1 after GRT labeling is denoted as M1* (panel H).

Figure 6. Comparison of oxidation patterns after 5 min in H_2O_2 followed by GRT labeling, (A) The carbonyl-depleted protein is dominated by M0 and M1*. Other oxidation peaks have very low intensity. (B) The carbonyl-containing population exhibits a dramatically elevated oxidation level. Peak maxima of oxidatively modified species are highlighted, annotation is as in Figure 5.

Figure 7. Top-down MS/MS data produced by CID of cyt c^{16+}. (A) Sequence with observed fragmentation sites. (B) Representative ion signals after fragmentation of M0 (unmodified protein, *m/z* 773.5, top row), M1 (first modification peak, center row, *m/z* 774.4), and M1* (first modification peak after GRT labeling, *m/z* 774.5). Peaks are labeled following standard *b* and *y* ion notation. Each panel also shows a simulated isotope distribution, corresponding to either the unmodified protein (circles) or the +O species (diamonds). The +O Da modification can be assigned to Y67. For information regarding the -NH_3 neutral loss from y_{56}, see Figure S14.

Figure 8. Proposed model for the H_2O_2-induced peroxidase activation of cyt *c*. MS-detected proteoforms are denoted along the top. Dotted lines in M0 and M1* indicate occasional opening of distal contacts due to protein conformational fluctuations, allowing for Fe-H_2O_2 interactions that are required for activation (oxygen incorporation into Tyr67, carbonylation of Lys_x). M1, M2, ... represent peroxidase-active species where Fe-H_2O_2 contacts are greatly facilitated because the distal coordination site is vacant. The nature of "Lys_x" could not be determined with absolute certainty in this study, but our data indicate that it corresponds to Lys72 and/or Lys73.

Figure 1

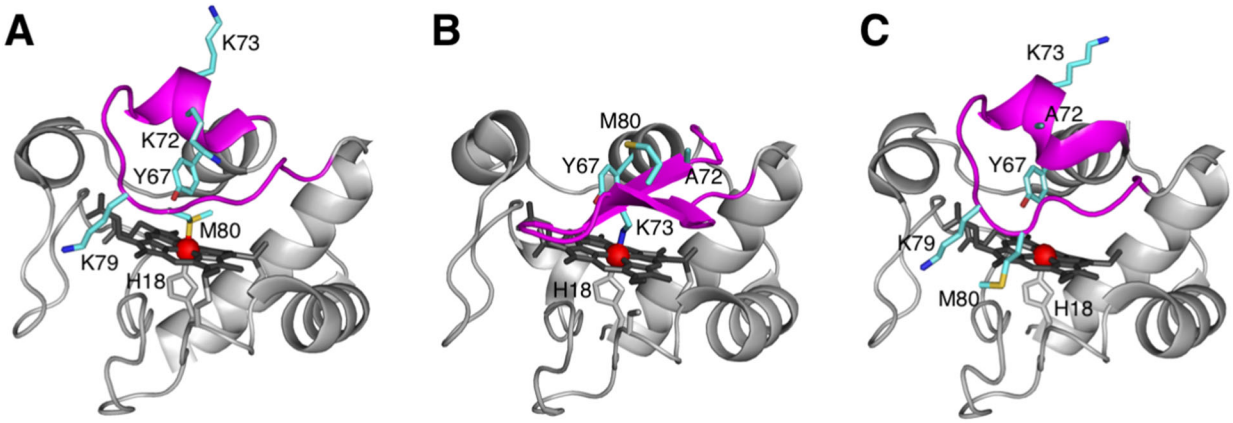

Figure 2

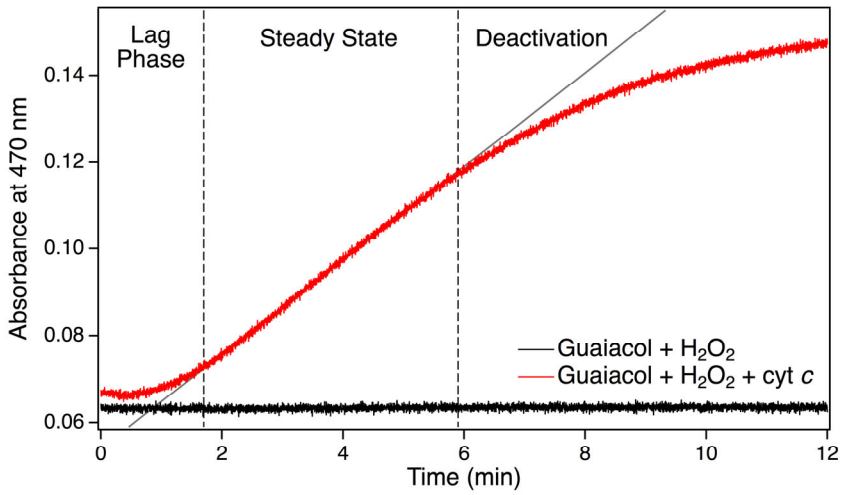

Figure 3

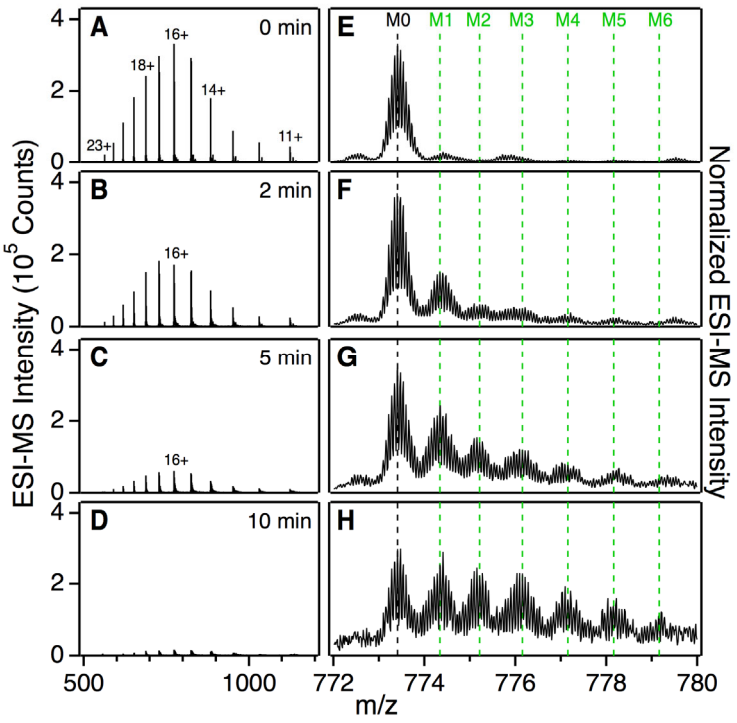
A
0 min
16+
18+
14+
23+
11+
B
2 min
16+
C
5 min
16+
D
10 min
E
M0
M1
M2
M3
M4
M5
M6
F
G
H
ESI-MS Intensity (10^5 Counts)
Normalized ESI-MS Intensity
0
2
4
500
1000
772
774
776
778
780
m/z

Figure 4

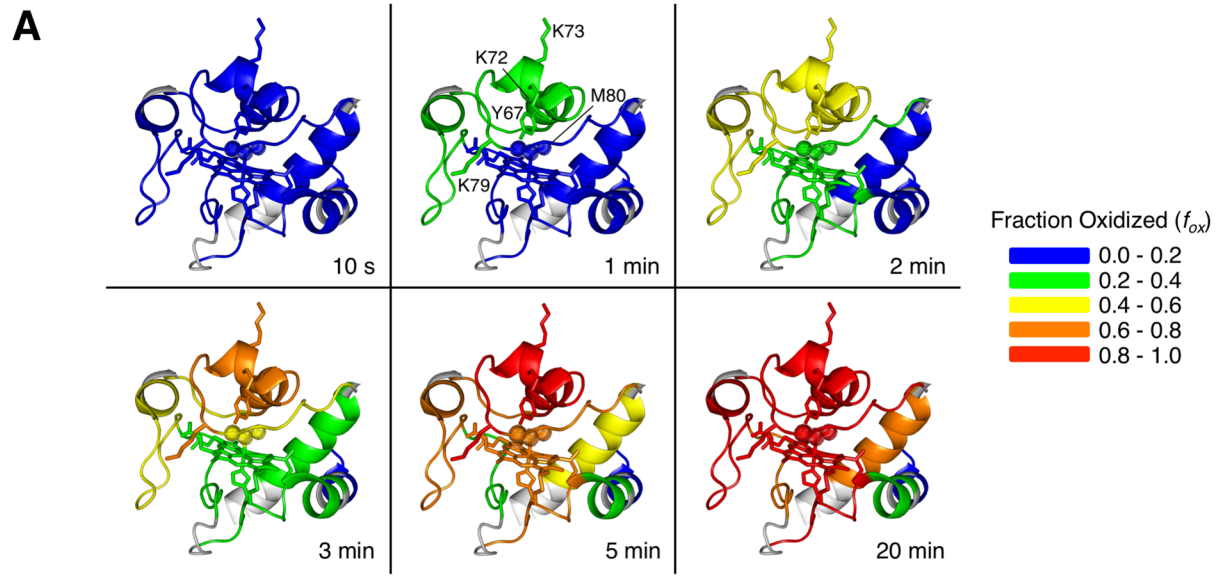

B

T1 T4 T5+heme T8 T9-10 T12

GDVEKGKKIF VQKCAQCHTV EKGGKHKTGP NLHGLFGRKT GQAPGFTYTD ANKNKGITWK

1 11 21 31 41 51

T13-14 T15 T16 T18-20

EETLMEYLEN PKKYIPGTKM IFAGIKKKTE REDLIAYLKK ATNE

61 71 81 91 101

Figure 5

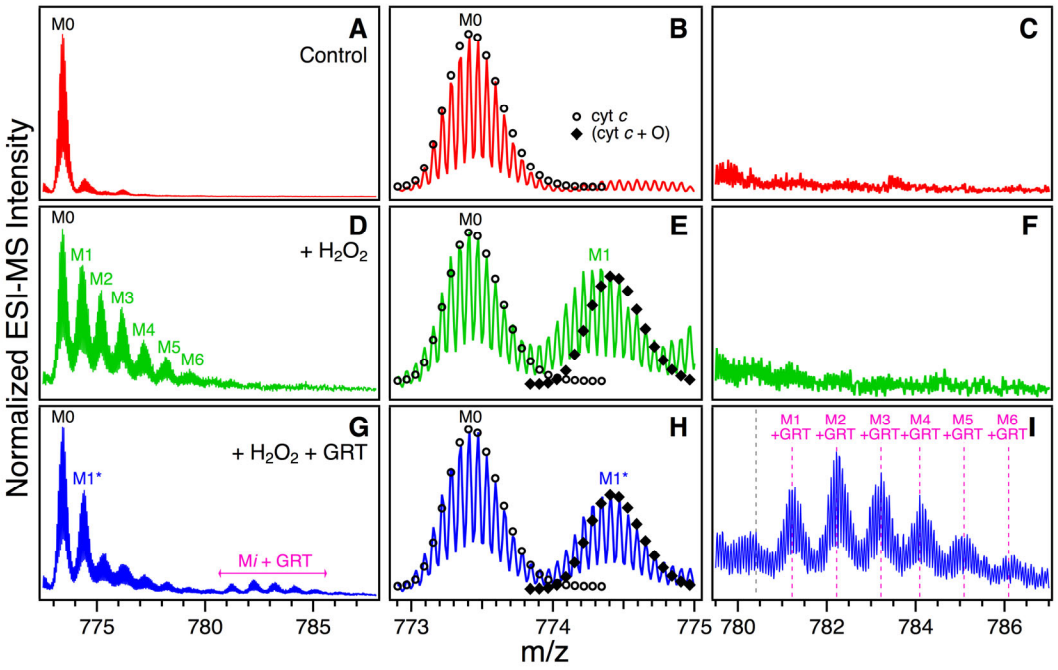

Figure 6

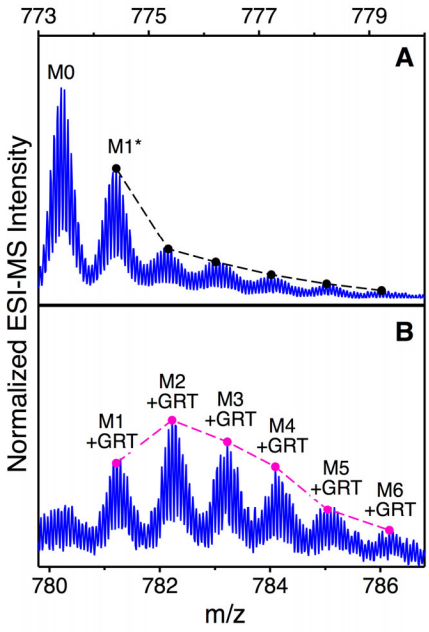

Figure 7

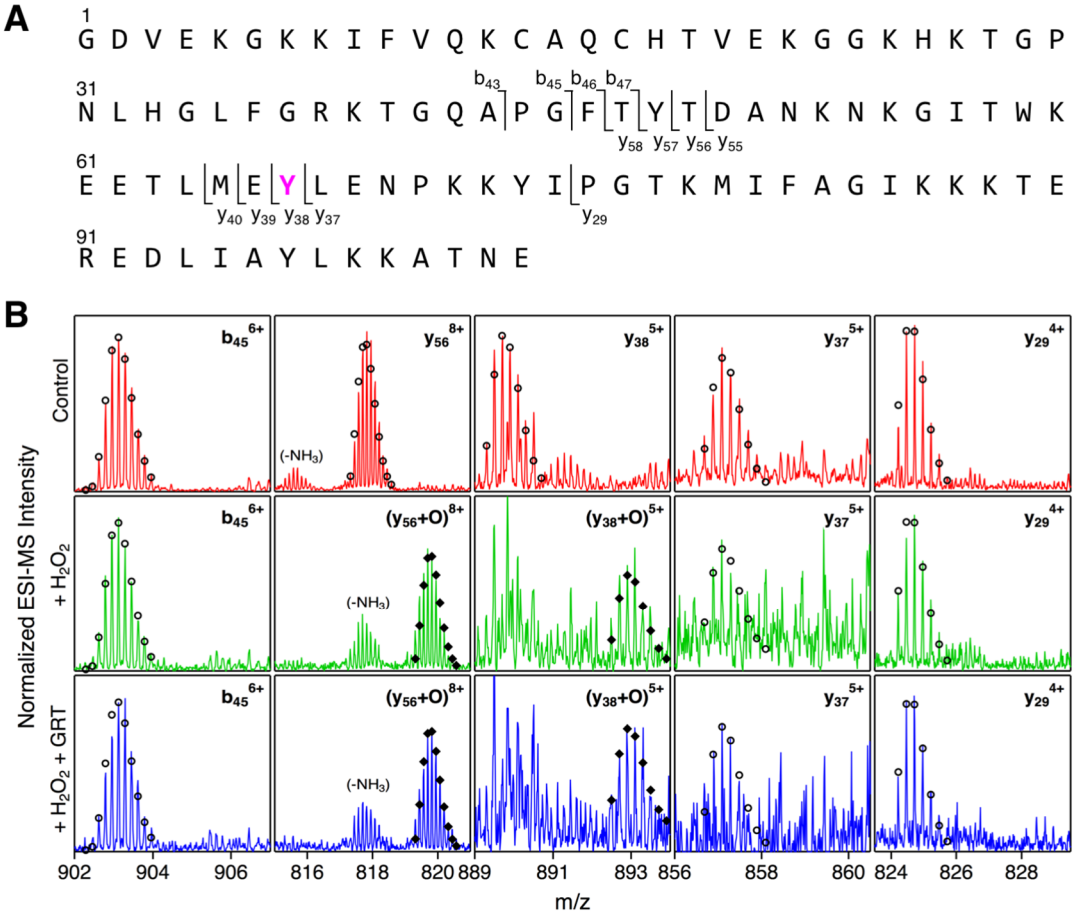
A
1
G D V E K G K K I F V Q K C A Q C H T V E K G G K H K T G P
31
N L H G L F G R K T G Q A P G F T Y T D A N K N K G I T W K
61
E E T L M E Y L E N P K K Y I P G T K M I F A G I K K K T E
91
R E D L I A Y L K K A T N E
b43 b45 b46 b47
y58 y57 y56 y55
y40 y39 y38 y37
y29
B
Control
+ H2O2
+ H2O2 + GRT
Normalized ESI-MS Intensity
b45 6+
y56 8+
y38 5+
y37 5+
y29 4+
(-NH3)
(y56+O) 8+
(y38+O) 5+
902 904 906
816 818 820
889 891 893
856 858 860
824 826 828
m/z

Figure 8

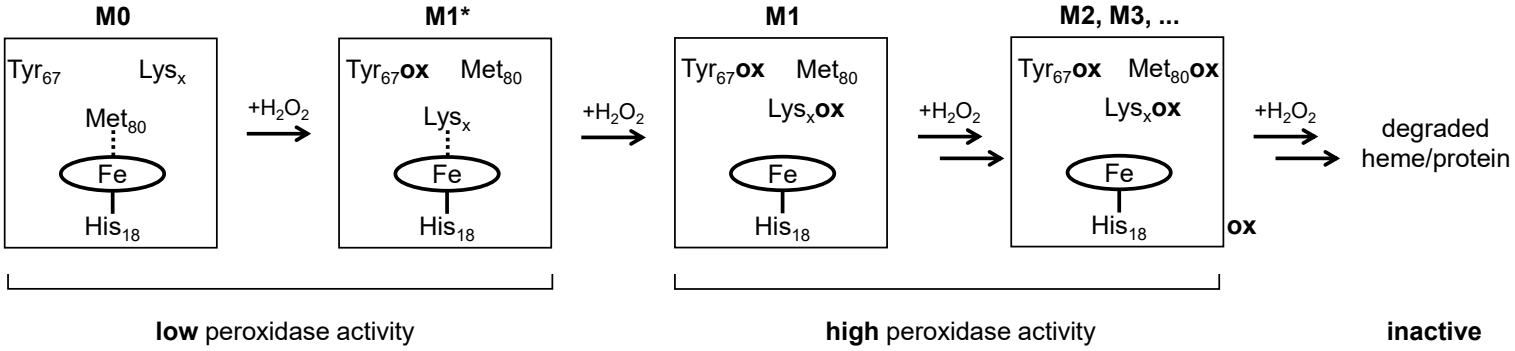
M0
M1*
M1
M2, M3, ...
Tyr67
Lysx
Met80
Fe
His18
+H2O2
Tyr67ox
Met80
Lysxox
Met80ox
ox
degraded
heme/protein
low peroxidase activity
high peroxidase activity
inactive

FOR TOC ONLY

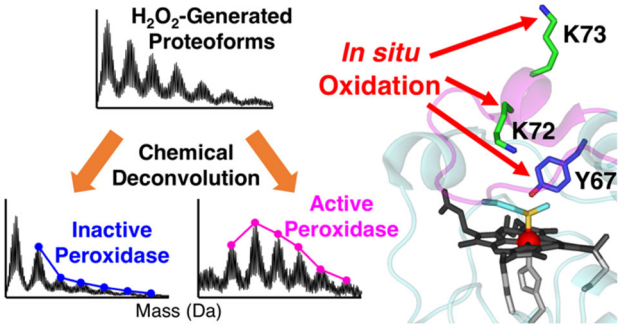
H_2O_2-Generated Proteoforms
Chemical Deconvolution
Inactive Peroxidase
Active Peroxidase
Mass (Da)
In situ Oxidation
K73
K72
Y67